Thermal vitrification in suspensions of soft colloids: Molecular dynamics simulations and comparison with experiments

A. N. Rissanou,[1,2] D. Vlassopoulos,[1,3] and I. A. Bitsanis[1,*]

[1]*Foundation for Research and Technology—Hellas, Institute for Electronic Structure and Laser, P.O. Box 1527, 711 10 Heraklion, Crete, Greece*

[2]*Department of Physics, University of Crete, 710 03 Heraklion, Crete, Greece*

[3]*Department of Material Science and Technology, University of Crete, 710 03 Heraklion, Crete, Greece*

(Received 24 September 2003; revised manuscript received 22 September 2004; published 14 January 2005)

Dense suspensions of multiarm star polymers are known to develop liquidlike microstructure, which has been attributed to the similarities between high functionality stars and colloidal particles interacting via soft, long ranged potentials. Recent experimental studies reported a counterintuitive solidification of suspensions with $f=128$, upon increase of the temperature in marginal solvents. We present our results from molecular dynamics simulations of dense suspensions of multiarm star polymers. Star polymers are modeled as "soft spheres" interacting via a theoretically developed potential of mean field. Our results show a transition towards a "glassy" state at a temperature very close to the one reported experimentally. The features of the transition are consistent with those of *ideal* glass transitions, as described by *ideal* mode coupling theory. Furthermore, our findings illustrate the road to vitrification for these soft-colloidal suspensions. Higher temperatures result in arm expansion that causes jamming and more than compensates for faster short time, temperature induced kinetics.

DOI: 10.1103/PhysRevE.71.011402 PACS number(s): 82.70.Dd, 64.70.Pf, 61.20.Ja, 61.25.Hq

I. INTRODUCTION

Star polymers consist of f linear polymer chains (usually referred to as "arms," while f is termed "functionality"), which originate from a compact central "core." The core dimensions are usually much smaller than the linear dimension of the arms [1]. The use of chlorosilane chemistry and anionic polymerization made possible the controlled synthesis of high functionality star 1,4-poly-butadienes [2,3]. These high functionality stars ("multiarm" star polymers) constitute an interesting class of materials with rich and often unexpected behavior, especially when suspended in liquids at high concentrations [4–6].

The material properties of dense multiarm star polymer suspensions originate from the interesting blend and interplay of polymeric and colloidal characteristics [6]. The internal structure of these macromolecules has been understood by means of concepts (e.g., self-similarity) and described by means of tools (i.e., scaling analysis and self-consistent mean field theory) central to polymer physics [7–9]. Multiarm star suspensions exhibit "liquidlike" ordering [10–13], and predictions suggest that they crystallize near their overlap volume fraction [9,14]. In fact, despite some indirect indications coming from NMR data [15], no unambiguous experimental evidence confirming the crystallization predictions for multiarm stars has been presented to date, other than some fragmental preliminary data [16]. However, recent progress on this front seems to support the crystallization scenario [17]. On the other hand, monodisperse suspensions of microgels or spherical particles with short grafted polymeric chains, as well as co-polymer micelles, are known to crystallize at sufficiently high concentrations [18–24].

In summary, a colloidal superstructure develops at the multistar level that can be analyzed and understood using the traditional tools of liquid-state theory [4,25]. However, this effort requires the development of accurate interstar potentials. Precisely at this step, the interplay between the colloidal and polymeric nature of multiarm stars becomes apparent.

The interstar potential [25] is a parametrized free energy, which involves a pre-averaging over certain classes of microvariables. In our problem these are associated with the solvent (and are already pre-averaged at the polymeric, i.e., intrastar level) as well as with arm conformations and the thermodynamic penalty of space sharing among arms belonging to neighboring stars.

The pair-potential function should depend on core-core distance (spherical symmetry). The potential parameters should be fully specified in terms of core linear dimension (a), arm degree of polymerization (N), star functionality (f), and temperature (T).

Two pair-potentials that meet the aforementioned requirements have been proposed during the past several years:

(i) A potential appropriate under good (literally athermal) solvent conditions [10], which is an interpolation between a Yukawa expression proposed by analogy to colloids (large interstar distances) and a logarithmic expression based on polymer physics arguments [8] (small interstar differences). The accuracy of this potential form has been confirmed directly by molecular dynamics simulations [26]. Its input to liquid-state theories has led to predictions that agree

*Author to whom correspondence should be addressed.

closely with small-angle neutron scattering (SANS) experimental data [10], and it has been used to chart theoretical phase diagrams of dense multiarm star suspensions [4,27].

(ii) A potential suitable under "near-Θ" or "marginal" solvent conditions. The starting point for the development of this potential form is the expression for the interaction between flat surfaces coated by grafted polymers, which is derived via a self-consistent field analysis [28]. Curvature effects are taken into account via the Derjaguin approximation [29]. The input of the latter potential to liquid-state theories has led to predictions that agree fairly well with the data from SANS experiments [11]. Unfortunately, there has been no direct molecular dynamics test performed on this potential, similar to the one in the good solvent case [26]. Furthermore, the accuracy of the Derjaguin approximation is questionable under the high curvature conditions inherent in the reality of a "tiny" core [30].

A striking example of the counterintuitive behavior that can result from the interplay between polymeric background and colloidal superstructure is the unexpected "gelation" upon heating recently observed in concentrated suspensions of multiarm star polymers [5,12,13]. The effect of temperature in inducing a liquid-solid transition was observed in a series of rheological measurements [Fig. 1(a)]. Dynamic temperature ramp tests indicated that the material response changed dramatically from liquidlike to solidlike. The frequency spectra showed that at lower temperatures the star polymer solution exhibits viscous liquid behavior ($G' \sim \omega^2, G'' \sim \omega, G'' > G'$), whereas upon heating it turns into a weak elastic solid ($G' > G''$ and both moduli exhibit a very weak frequency dependence), accompanied by an increase in the values of the moduli by several orders of magnitude. At temperatures above the liquid-solid transition the intermediate scattering function (determined by DLS measurements) exhibited a slow "cluster" mode, typical of glasses [Fig. 1(b)] (in addition to the standard cooperative and self-diffusion modes). This mode melted upon cooling to the liquid regime (typically after 10 h in experiments [5]). PFG NMR experiments [15] distinguished the glass region by the fact that the incoherent structure factor exhibited a kinetic arrest at long times.

The value of q in Fig. 1(b) is 0.033 nm^{-1} and reflects multistar packing. The peak of the structure factor was located at 0.13 nm^{-1}, as determined (roughly) by SANS experiments [5]. It should be mentioned that the polymeric nature of arms is present in experimental considerations of this type, while absent in our "soft-sphere" modeling. In real multiarm star polymers the form factor has a density dependence, which complicates comparisons with "effective particle" simulations. Figure 1(a) depicts the transition from liquidlike to solidlike dynamics. The data of Fig. 1(a) refer to nominal volume fractions that range from less than 1.00 to 1.83 [53].

The main objective of this paper is to investigate, by means of molecular dynamics simulations, the temperature induced changes in colloidal superstructure and star dynamics *under marginal solvent conditions*. To this end, multiarm star polymers are modeled as (structureless) soft spheres interacting via potential (ii) mentioned above. From a different perspective this study constitutes a rather demanding test of potential (ii) and of its capacity to capture the basic changes associated with experimentally observed phenomena.

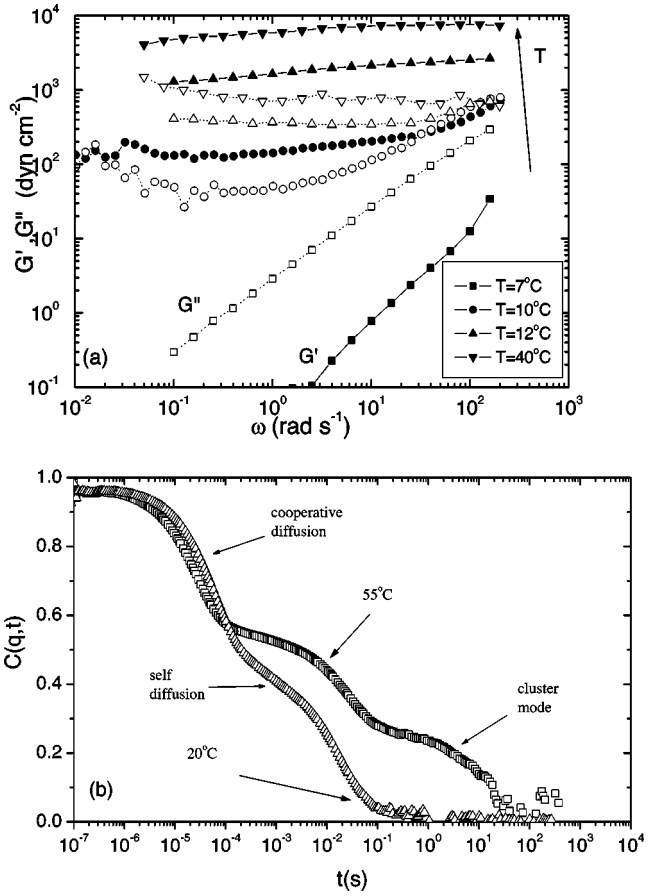

FIG. 1. (a) Dynamic frequency sweeps of 12 856/decane 6.9 wt % solutions indicating the liquid-solid transition (G': solid symbols; G'': open symbols) [53]. (b) Dynamic light scattering data on the intermediate scattering function, which show the three step relaxation at $T=55\,^{\circ}C$ [12].

The rest of this paper is organized as follows: Details about the interaction potential and the simulation method are given in Sec. II. Section III contains the main body of our findings. These findings and their relevance, or lack thereof, to the experimentally observed phenomena are discussed in Sec. IV. Finally, Sec. V contains our concluding remarks.

II. SIMULATION MODEL AND METHOD

As mentioned earlier, we model each star polymer as a "soft sphere" whose size increases with temperature. The interaction between particles is quantified by the temperature dependent pair potential (ii) which is given by the following formula [11,29]:

$$\beta V(r) = \begin{cases} \infty & r < 2a \\ U_0\left[-\ln y - \frac{9}{5}(1-y) + \frac{1}{3}(1-y^3) - \frac{1}{30}(1-y^6) \right] & 2a < r < 2(a+L) \\ 0 & 2(a+L) < r \end{cases}, \tag{2.1}$$

$$\beta = 1/k_B T, \quad y = \frac{r-2a}{2L}, \quad U_0 = \frac{\pi^2 L^3 f}{48 N l^2 a}, \quad L \approx R_0 - a$$

a is the "core" radius of the star, R_0 is a measure of the unperturbed star radius, f is the star functionality, N is the number of "monomers" per chain and l is the "monomer length."

For purposes of comparison with experimental findings [5] potential parameters were chosen to correspond to 1,4-poly-butadiene stars with $f=128$ and arm molecular weight 56 000 amu dissolved in decane. The temperature interval examined was 15–55 °C. However, we focus on the results for four temperatures (35, 45, 50, and 55 °C), as this temperature interval coincides approximately with the interesting transition region. Both experimental evidence and theoretical considerations indicate that decane is a marginal solvent for these poly-butadiene stars over the entire range of temperatures studied (this point is further discussed below).

The assignment of values to the parameters of Eq. (2.1) is a delicate issue. l should be viewed as the persistence length (estimated to be 0.66 nm for 1,4-poly-butadiene) and N as the number of subunits containing enough monomers to encompass one persistence length [11] (an equivalence based on "Kuhn segments" would hardly affect the results). The effective core radius a does not coincide necessarily with the radius of the dendritic core. If the quantity $lf^{1/2}$ exceeds the radius of the dendritic core, a should be identified with that latter size [7], which is indeed the case in our systems and $a=lf^{1/2}=7.5$ nm. It should be noted that the outermost part of the potential is relatively insensitive to the exact value of a. According to the self-consistent field approach [28], R_0 is the distance (from the star geometrical center) beyond which the polymer concentration vanishes. It was approximated by the measured value [5] of the hydrodynamic star radius R_{H} under high dilution. R_{H} is sensitive to the outermost portions of the polymer layer. It constitutes a better approximation to R_0 than other measures of the star linear dimension (e.g., R_{g}), *in marginal solvents, when the self-consistent field approach supplies the basis for the interstar potential*. Furthermore, experimental evidence suggests that R_{H} is preferable over other measures of the linear dimension for scaling dynamical properties, e.g., self-diffusion [31].

TABLE I. Experimental values for the hydrodynamic radius (column 2) at various temperatures, effective volume fractions (column 3).

T (°C)	$R_H(nm)$	ϕ/ϕ^*
15	36.9	0.770
20	37.8	0.828
25	37.8	0.828
30	38.4	0.868
35	38.8	0.895
40	39.8	0.966
45	40.7	1.033
50	42.4	1.168
55	44.3	1.332

The experimental values of the hydrodynamic radii used in our simulations are listed in Table I. The third column of Table I contains the effective volume fractions (ϕ/ϕ^*) of the star polymer suspensions ($\phi^*=[4\pi R_H^3(T)/3]^{-1}$).

The potential of Eq. (2.1) is plotted in Fig. 2 for several temperatures. This potential is compared with a purely repulsive (truncated-shifted) Lennard-Jones (LJ 12-6) potential. The parameters of the LJ potential were determined on the basis of the "hard sphere equivalence" between the potential of Eq. (2.1) and the truncated-shifted LJ potential. The softness and the slow decay of the interstar potential are depicted clearly in Fig. 2. Many interesting features of dense multiarm star suspensions originate from the ultrasoft nature of the interstar potential. In particular, the astonishingly high values of the effective volume fraction are a direct consequence of potential softness.

Regarding the specifics of the simulations, the number density was fixed to its experimental value [5] of 3.66×10^{15} stars/cm^3. The effective volume fraction ranged from 0.77 to 1.33 over the temperature range studied (15–55 °C).

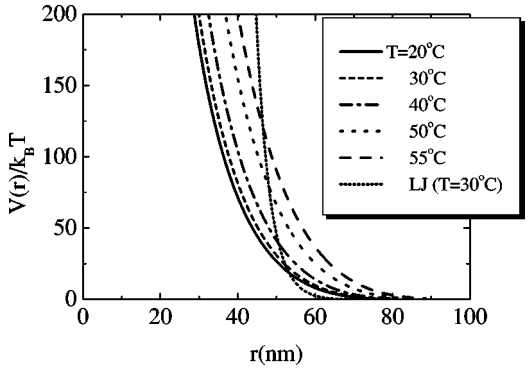

FIG. 2. Comparison of the interstar potential for five different temperatures between 20 and 55 °C with the truncated-shifted Lennard-Jones potential at $T=30$ °C.

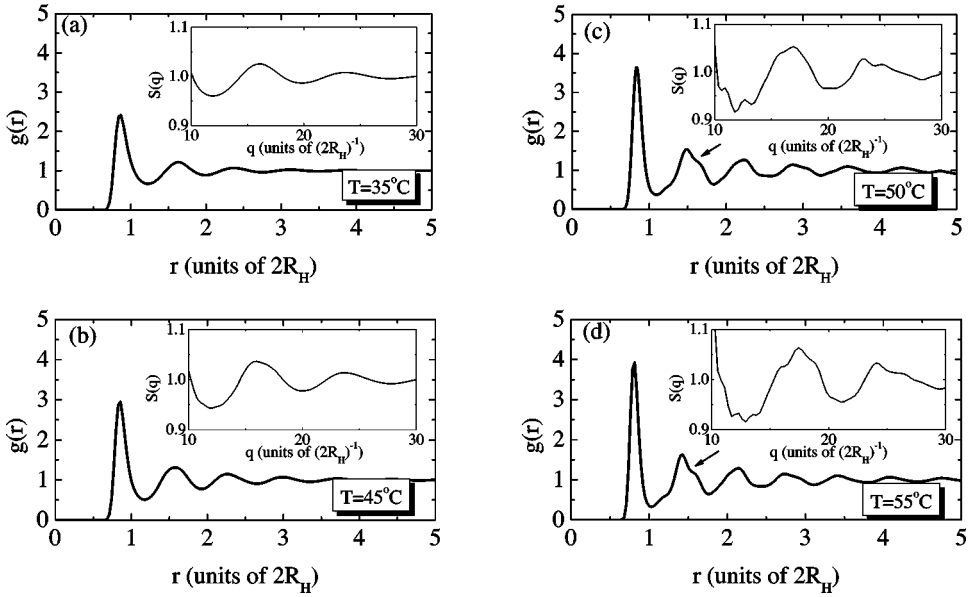

FIG. 3. Radial distribution function for temperatures varying from $T=35$ to $T=55\,^{\circ}\mathrm{C}$. Inset: corresponding structure factor in magnification to the second and third peaks where interesting features appear.

All systems simulated contained 2916 "soft spheres." The side of the periodic box was about 1 μm, which is 20–25 times larger than R_{H} (depending on T). The temperature-induced densification of the system resulted solely from the expansion of star polymers (i.e., soft spheres) through the increasing value of R_0 (i.e., R_{H}).

After charting the parameter space explored by our simulations, it is imperative to justify quantitatively the usage of potential (ii). Our best estimate for the Θ temperature [11] is $27\,^{\circ}\mathrm{C}$. The emergence of a "swollen blob" regime within each star polymer requires [7]

$$N \gg f^{1/2}\upsilon^{-2} = f^{1/2}(1-\Theta/T)^{-2}, \tag{2.2}$$

where N is the number of Kuhn segments and υ the excluded volume of the statistical segment. c_∞ is about 5 for polybutadiene [32], which leads to a value of N close to 200 for 56 000 amu arms. For $f^{1/2}\upsilon^{-2}\approx 10^4$ at $35\,^{\circ}\mathrm{C}$ and $f^{1/2}\upsilon^{-2}\approx 1500$ at $55\,^{\circ}\mathrm{C}$, the Daoud-Cotton criterion for the existence of the swollen blob regime is never even approached. Therefore the star polymers in the systems studied in this work consist of a central core and an outermost portion of *unswollen* blobs, i.e., the entirety of the chain backbone (except the short central parts, which form the core and are at melt state) experiences marginal solvent conditions. The self-consistent-field approach is appropriate and the major reservations on potential (ii) relate to the accuracy of the Derjaguin approximation for stars with a minute, highly curved core.

Constant temperature (canonical ensemble) molecular dynamics (MD) was the method used in all simulations presented here. Standard (N,V,T) Metropolis Monte Carlo was inefficient in probing the configuration space of dense systems in the verge of jamming, like those studied in this work, as it required the use of an extremely small attempted displacement comparable with the natural displacement of the "deterministic" system during a MD time step.

Temperature was kept constant by means of mild velocity scaling (every 30 time steps). The equations of motion were integrated by means of the (velocity) Verlet algorithm. All systems were initiated from amorphous configurations. Equilibration was monitored following the time change of the total energy and the temporal evolution of the radial distribution function. After equilibration, production runs ranged from 10^5 (low T) to about 2×10^6 MD steps (high T).

Preliminary simulations on monodisperse multiarm star suspensions indicated a slow "aging" of the amorphous solid towards a more ordered structure. It has been pointed out that a certain degree of complexity is necessary to keep a system in a metastable amorphous state [33,34]. Indeed, size and arm dispersity are about 10%, for the experimentally used multiarm star 1,4-polybutadienes [2,3,35]. A 10% dispersity in R_0 (drawn from a uniformly random distribution) was sufficient to stabilize the amorphous state for the duration of the simulations.

Clearly, MD results in an unphysical short time ballistic motion of soft spheres. Any realistic description of short-time motion would require Brownian dynamics simulations with the correct hydrodynamics, i.e., hydrodynamic interactions and a proper version of the "lubrication approximation" for "porous" objects (like our soft spheres), as well as an established theory of "arm diffusion," which would supply an effective friction coefficient. However, *the objective of this work is to study the main trends in long time particle dynamics and specifically in situations, where long and short time dynamics are, largely, decoupled* [27,36]. This justifies the use of MD on the grounds of convenience and computational efficiency. Studies on purely repulsive ultradense LJ systems support this point of view [37]. The decoupling of short and long time dynamics is a subtle issue [36], which will be further discussed in Sec. IV.

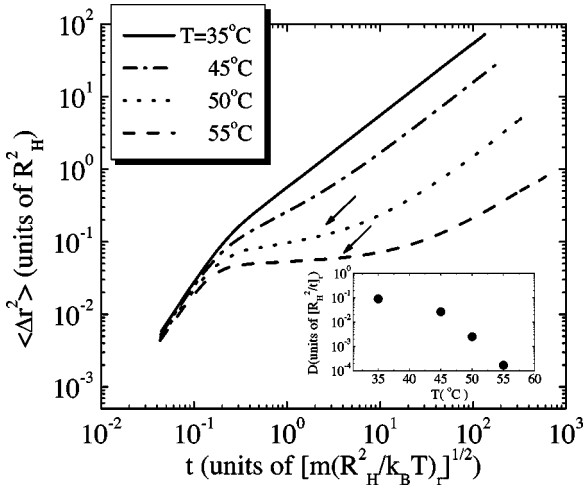

FIG. 4. Mean squared displacement as a function of time for temperatures between $T=35\,^{\circ}\mathrm{C}$ and $T=55\,^{\circ}\mathrm{C}$. Plateaus are evidence of "caging effects" at high temperatures. Inset: long-time self-diffusion coefficient at four temperatures (35, 45, 50, 55 °C).

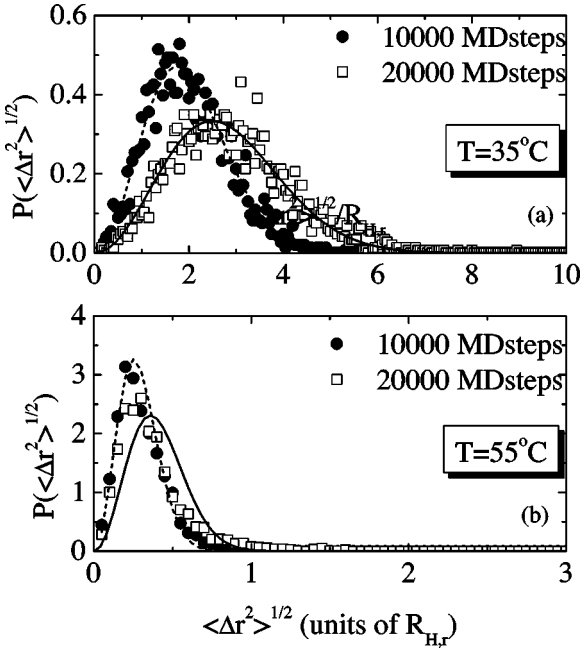

FIG. 5. Distributions of particle displacements for two different time instants (10 000, 20 000 MD steps) and for two temperatures $T=35\,^{\circ}\mathrm{C}$ and $T=55\,^{\circ}\mathrm{C}$. Solid lines signify the time evolution of a Gaussian distribution according to Eq. (3.1).

III. RESULTS

Figure 3 contains our MD results for the radial distribution function of the soft-spheres suspensions at four temperatures. Typical liquidlike ordering [10,11] is manifest at the lowest temperature (35 °C). Therefore the number density is sufficiently high to induce local "packing" of the soft spheres (stars) and the development of interstar microstructure similar to that of dense liquids of spherically symmetric molecules (and that of dense suspensions of "hard" colloids). At 45 °C the structure remains liquidlike but the oscillations sharpen. More interesting are the features that first appear at 50 °C and develop further at 55 °C. The gradual split of the second peak, the steady development of a "shoulder" (incipient split) of the third peak and the flattening of the fourth peak are precursors of a crystalline (fcc) structure. Such microstructural changes reflect the uneasy competition between a "frozen" crystalline state and a "mobile" amorphous state. These interesting features are often indicative of vitrification. Similar, although less pronounced, features appear in the structure factor (insets of Fig. 3) and could, in principle, be detected experimentally.

The above observations render necessary the monitoring of soft sphere mobility. The mean square displacements of soft spheres vs time are depicted in Fig. 4. It should be noted that very short time features ($t<0.5$ in Fig. 4) result, at least partially, from the inherent "ballistic" trend of MD. The linear time dependence, typical of Fickian diffusion, is very clear at 35 °C (and below 35 °C, not shown in Fig. 4). A weak shoulder, indicative of a slight delay at intermediate times can be seen in the $T=45\,^{\circ}\mathrm{C}$ curve. The situation is more interesting at higher temperatures. At 50 °C and, in a stronger fashion, at 55 °C the short range mobility is followed by a pronounced stagnation, which persists for two decades in the time scale of Fig. 4. Soft-sphere mobility recovers only at much longer times and the resulting self diffusivity is substantially lower (by two orders of magnitude) than that observed in the liquid suspension ($T \leqslant 35\,^{\circ}\mathrm{C}$). The long-time self-diffusion coefficient (inset of Fig. 4) also illustrates the dramatic slow down of soft-sphere self-diffusion upon approaching the jamming temperature. This type of time evolution of the MSD curves is characteristic of "caging," i.e., the temporary confinement of particles in cages formed by their immediate neighbors [38,39].

The non-Fickian nature of soft-sphere mobility at high temperatures and intermediate times is also apparent in Fig. 5, where histograms of particle mean square displacements and their time evolution (self-part of the van Hove correlation function) are plotted at $T=35\,^{\circ}\mathrm{C}$, and $T=55\,^{\circ}\mathrm{C}$. Fickian diffusion requires that the probability density for particle (mean square) displacements spreads out with time according to the next formula, which is plotted with lines in Fig. 5,

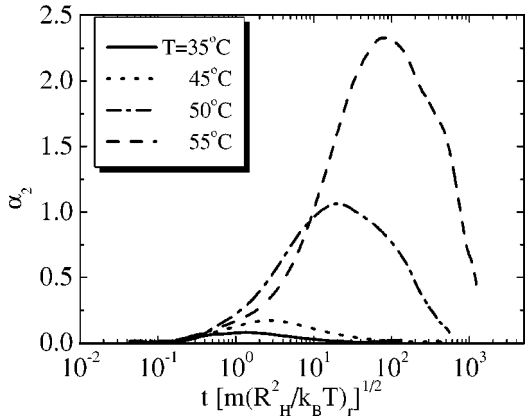

FIG. 6. The time evolution of the non-Gaussian parameter (35–55 °C).

$$P(\langle \Delta r^2 \rangle^{1/2}) = \frac{4\pi \langle \Delta r^2 \rangle}{8(\pi D t)^{3/2}} \exp(-\langle \Delta r^2 \rangle / 4Dt). \quad (3.1)$$

The van Hove curves are Gaussian and their time evolution follows Eq. (3.1) at $T=35\,^\circ$C. Strong discrepancies from the Fickian pattern are clear at the highest temperature studied ($T=55\,^\circ$C). The van Hove correlation function spreads at a rate considerably slower than that predicted by Eq. (3.1). Furthermore, even the distribution of particle displacements at a fixed time does not follow the Gaussian statistics implicit in Eq. (3.1). It should be pointed out that the time intervals for the particle displacements shown in Fig. 5 were selected to be in the plateau of the mean square displacement curves of Fig. 4. This choice illustrates that particles do not diffuse according to the Fickian prescription at intermediate time scales.

The "non-Gaussian" parameter, $a_2(t)$ defined below, is the simplest measure of deviation from Gaussian statistics,

$$a_2(t) = \frac{3\langle r^4(t) \rangle}{5\langle r^2(t) \rangle^2} - 1. \quad (3.2)$$

Equation (3.1) implies that the non-Gaussian parameter vanishes. Any deviations of this quantity from 0 are indicative of non-Gaussian spread of particle positions and, in our case, of non-Fickian diffusion. Figure 6 contains our simulation data on the non-Gaussian parameter. Clearly, soft-sphere kinetics does not conform to the Fickian pattern for temperatures higher than 45 °C. This is manifested by the large values of $a_2(t)$. A comparison with Fig. 4 is illuminating. For the two highest temperatures the maxima in Fig. 6 occur at about the same time as the end of the plateaus ("α relaxation") in Fig. 4. The non-Gaussian parameter returns to 0 at long times signaling the re-emergence of Fickian diffusion, albeit at a rate 1–2 orders magnitude lower than that at 35 °C.

Experimentally, the incoherent structure factor (S_{inc}) can monitor particle displacements and detect deviations from Fickian kinetics. The expected superposition of S_{inc} vs q^2t is very satisfactory at 35 °C (Fig. 7). Discrepancies appear already at $T=45\,^\circ$C, which are certainly of the same origin as the weak shoulder in the mean square displacement curve of Fig. 4. At higher temperatures the superposition fails completely. Similar behavior, in similar suspensions, has been reported in the experimental findings of Ref. [15], albeit in a somewhat different context. These are strong trends detectable by PFG NMR [15].

Figure 8 contains a portion of a soft-sphere trajectory at $T=50\,^\circ$C. This is a typical trajectory. The caging effect is obvious. Substantial displacements are rare and occur abruptly. soft spheres move in a narrow region and effectively vibrate in their cells, until they manage to escape by jumping into a different cell, where they will be trapped again for a considerable time interval. Trajectories of this type constitute the physical basis for the plateau of the MSD curves at 50 and 55 °C.

There is abundant evidence that the escape from "cages" does not take place in a purely random, uncorrelated fashion. There exist small groups of neighboring soft spheres, which move cooperatively in the same region, performing jumps from one cage to another, as depicted in Fig. 9. It should be stressed that the trajectories shown in Fig. 9 are spatially correlated, i.e., the soft sphere centers are as close as depicted in Fig. 9. Such groups of particles can be thought of as "dynamical clusters." Correlated soft sphere trajectories, like those depicted in Fig. 9, supply concrete images of the physics captured by the self-consistent treatment of "in-cage" motion and cage formation breakdown in the context of ideal mode coupling theory [33,40].

Glotzer and co-workers [39] have proposed a more systematic way for examining this type of clustering. It involves the calculation of a displacement-displacement pair-correlation function $g_u(r;\Delta t)$ (the full definition in a *NVT* ensemble was developed in Ref. [39]),

$$g_u(r;\Delta t) = \int dr' \langle [u(r'+r,t,\Delta t) - \langle u \rangle] \times [u(r',t,\Delta t) - \langle u \rangle] \rangle, \quad (3.3)$$

where $u(r,t,\Delta t) = \Sigma_{i=1}^{N} \mu_i(t,\Delta t)\, \delta[r - r_i(t)]$ and $\mu_i(t,\Delta t) = |r_i(t+\Delta t) - r_i(t)|$.

This quantity would be identical to the radial distribution function $g(r)$, if displacements were statistically equal for all particles, as in the case of a regular liquid. If, however, particles, which at $t=0$ were separated by a distance r (e.g., a "tagged" particle and its nearest neighbors, or particles belonging to a transient "cluster") move in a correlated fashion over a time period Δt, the degree of this correlation will be quantified by $g_u(r;\Delta t)$. A comparison between $g(r)$ and $g_u(r;\Delta t)$ for a "typical" Δt (i.e., during the time period when their differences are apparent) is shown in Fig. 10. The most pronounced difference appears at the first maximum of $g(r)$, i.e., the strongest displacement-displacement correlation exists between a "tagged" particle and its first cell neighbors, which form its cage. Another interesting strong correlation exists among the tagged particle and its outermost second cell neighbors (shoulder of the second oscillation of g and g_u). Apparently, slight rearrangements of second neighbors play a crucial role in cage formation and dissolution. Finally, an excess correlation of displacements (g_u) over structural features (g) persists over several particle diameters.

The range of these excess correlations could be used as a measure of the dynamical cluster size. "Cluster rigidity," properly quantified, should be taken into account in the definition of dynamical clusters. Nevertheless, the issue of dynamical clusters is a central one. Whether it can be appropriately studied by simulations of this scale ($\sim$3000 particles) will be discussed in Sec. IV.

The excess correlation $\Gamma(t,\Delta t)$, as a function of Δt (inset of Fig. 10) is defined in Eq. (3.4a). The time dependence of this quantity (total excess correlation A) is defined in Eq. (3.4b) and our simulation data on it are shown in Fig. 11.

$$\Gamma(r,\Delta t) = [g_u(r,\Delta t)/g(r)] - 1, \quad (3.4a)$$

$$A \equiv \int dr \Gamma(r,\Delta t). \quad (3.4b)$$

The maximum of A sets a characteristic time (Δt^*) for displacement-displacement correlations (the point marked in

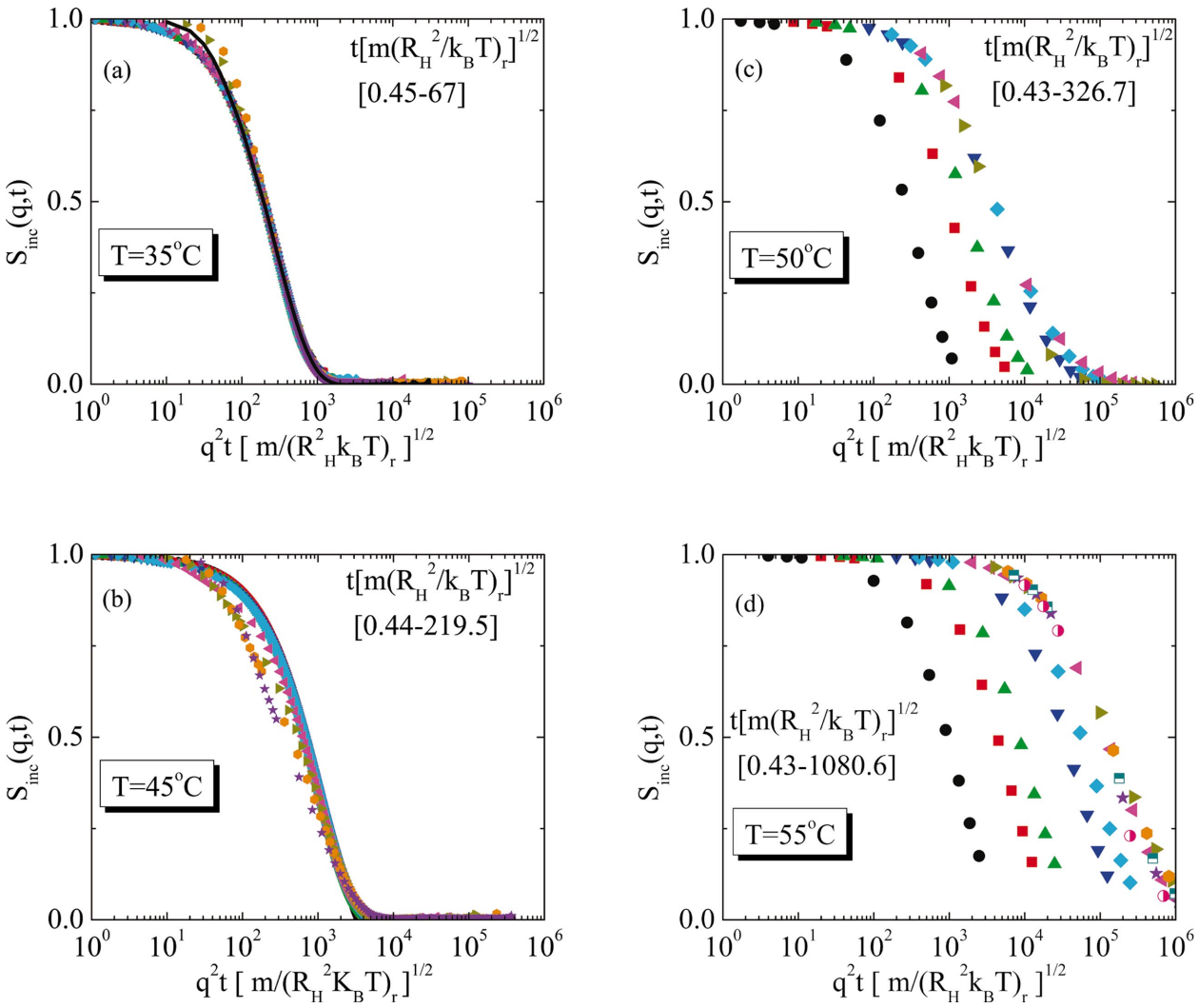

FIG. 7. (Color) The incoherent structure factor vs q^2t at four different temperatures (35°C, 45°C, 50°C, 55°C). t values increase from left to right.

a square box indicates the Δt used in Fig. 10, which is of the same order of magnitude as Δt^*. This time exceeds (by about a decade) the end of the plateau in the MSD curves (Fig. 4). *One is tempted to interpret* Δt^* *as the time when correlated escapes from cages (e.g., Fig. 9) take over and re-establish Fickian diffusion.*

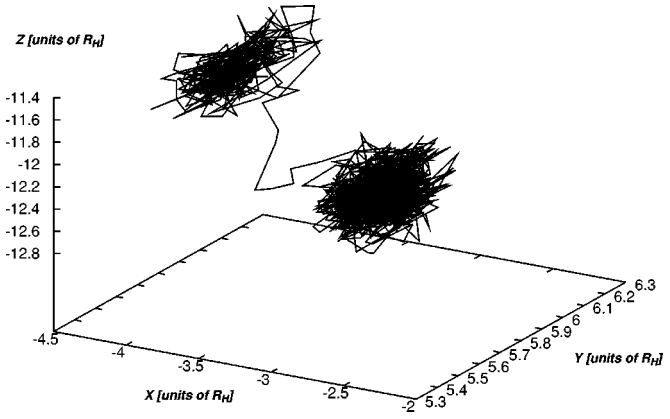

FIG. 8. Typical trajectory of one star at $T=50$°C. Jump from one cage to another.

A direct comparison with the experimentally determined frequency dependence of G' and G'' would be very interesting. Theoretically these calculations are straightforward [41]. However, the statistics of our data do not allow such comparisons.

The overall picture indicates that weak structural changes (like those depicted in Fig. 3) are accompanied by very strong qualitatively different effects on soft-sphere dynamics. In particular, the MSD curves illustrate clearly the separation between short and long time dynamics (the plateau in Fig. 4 extends over two decades in time), i.e., the caging effect. It is tempting therefore to examine dynamical changes taking place above 45°C, in ways suggested by ideal mode coupling theory (MCT) [33,40,42,43]. In this work we do not attempt a comprehensive and quantitative comparison with MCT predictions.

Figure 12 contains the simulation data for S_{inc} vs T at the four temperatures depicted in Fig. 4 (MSD's). The featureless behavior at 35 and 45°C is followed by a clear two step relaxation at 50 and 55°C, a manifestation of temporary

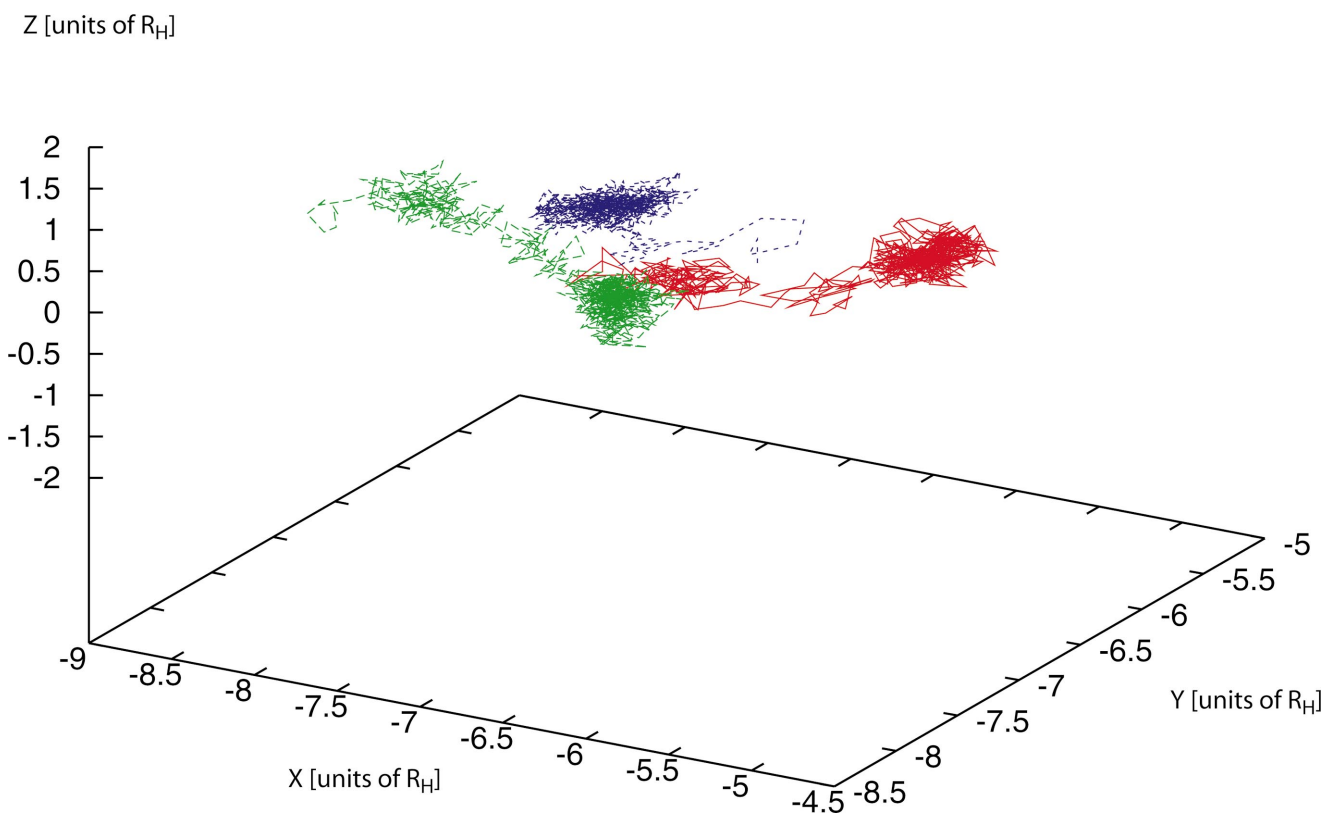

FIG. 9. (Color) Trajectory of an "effective dynamical cluster" with three stars at $T=55\,^{\circ}\mathrm{C}$ (cooperative motion).

structural arrest in the approach towards a nonergodicity transition. Sufficiently close to the nonergodicity transition the slow relaxation of $S_{\mathrm{inc}}(t)$ conforms to the von Schweidler power law series,

$$S_{\mathrm{inc}}(t) = f^{s}(q) - h^{(1)}(q)(t/\tau)^{b} + h^{(2)}(q)(t/\tau)^{2b} + O(t/\tau)^{3b}. \tag{3.5}$$

In the above equation $f^{s}(q)$ is the nonergodicity parameter, b is known as the von Schweidler exponent, and τ is a characteristic time associated with the α relaxation. The data in Fig. 12 conform to Eq. (3.5) at the two highest temperatures. The fits to Eq. (3.5) (dashed lines in Fig. 12) were done *for fixed* (i.e., q-independent b and τ). The relaxation time τ increases by more than three orders of magnitude from 50 to 55 °C, which indicates that the ideal glass transition point should be very close to 55 °C ($\tau_{50}\approx 1$, while $\tau_{55}\approx 1800$). Furthermore, the von Schweidler exponent was found to be 0.48, which is slightly, yet not negligibly, lower than that of hard sphere glasses (0.53) [44].

The Gaussian approximation on $S_{\mathrm{inc}}(q;t)$ and $f^{s}(q)$ $(f^{s}(q)\approx\exp\{-q^{2}r_{l}^{2}/6\})$ allows the estimation of the "localiza-

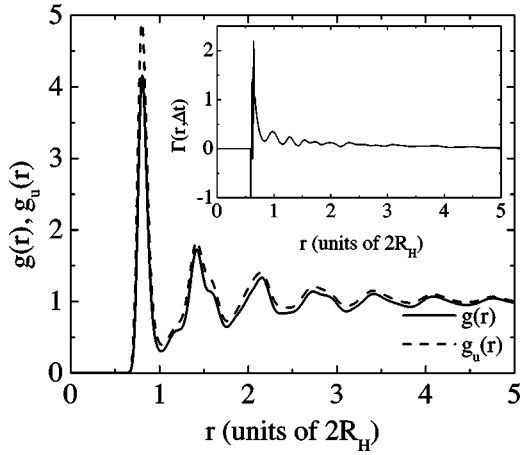

FIG. 10. The pair correlation function $g(r)$ and the "displacement-displacement" correlation function $g_u(r)$ vs r at $T=55\,^{\circ}\mathrm{C}$. Inset: the excess correlation Γ vs r.

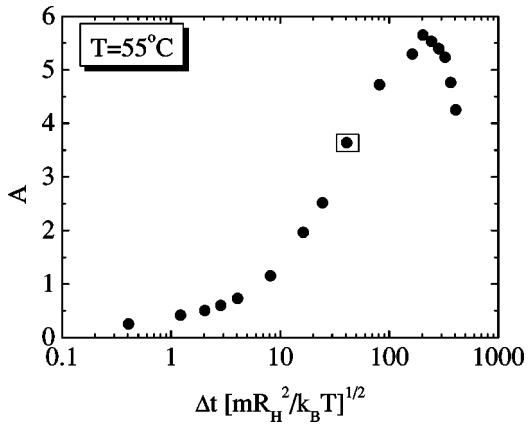

FIG. 11. The total excess correlation A as a function of Δt at $T=55\,^{\circ}\mathrm{C}$. The value in the square corresponds to the Δt used for the comparison between $g(r)$ and $g_u(r)$ in Fig. 10.

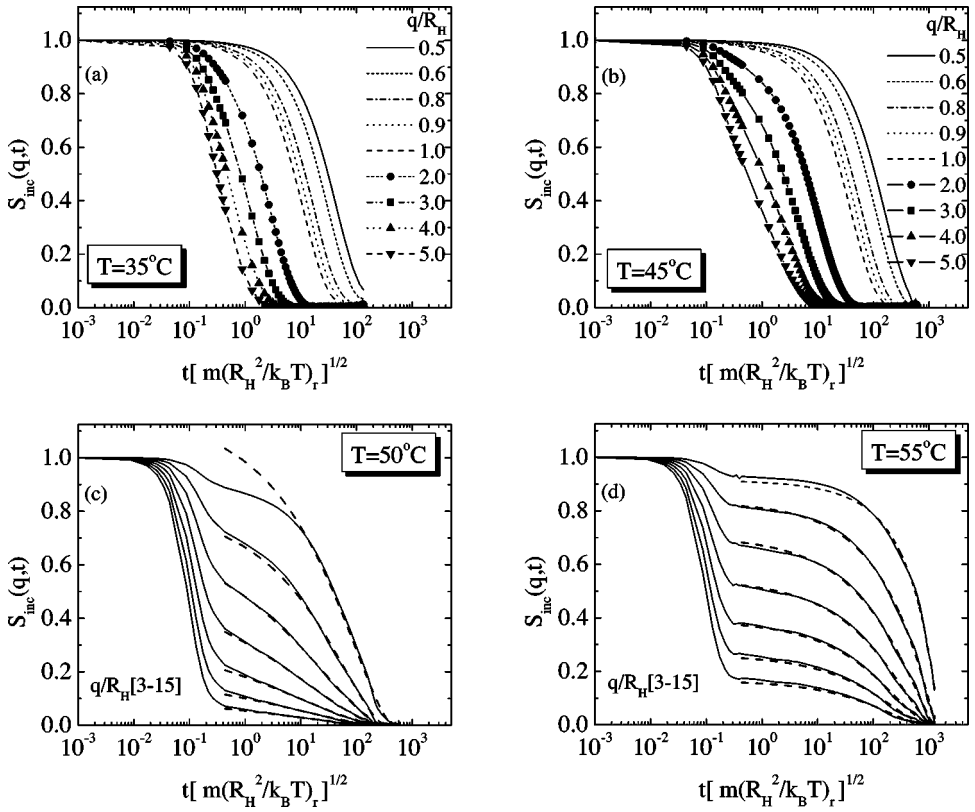

FIG. 12. The incoherent structure factor vs t at various q-values and at 4 different temperatures (35, 45, 50, and 55°C). Dashed lines at 50 and 55°C are fits according to Eq. (3.5). The q values at 50 and at 55°C increase from up to down with step 2.

tion length" (r_l), which quantifies the extent of *in-cage* soft sphere displacements. Although the quality of the approximation deteriorates for large wave vectors and close to the ideal glass transition temperature [38], the Gaussian approximation does supply an estimate of r_l. This comparison is shown in Fig. 13(a) for the highest temperature studied (55°C). The estimate for r_l is $0.215R_H$. The two values from the plateau in Fig. 13(b) and the fit of the nonergodicity parameter in Fig. 13(a) agree to within the second decimal with each other. Furthermore, they are both very close to the more accurate estimate supplied by the value of the plateau in the MSD curve of Fig. 4 (about $0.24R_H$). These values are higher than the corresponding hard sphere value ($0.14R$) [42,45], which is reasonable because the soft spheres in this study are less strongly localized at intermediate times, close to the glass, than the hard spheres.

IV. DISCUSSION

In this paper we present a MD study of the kinetic arrest of multiarm star polymers under marginal solvent conditions upon increasing T. MD was found to be more efficient than stochastic methods, in general, and BD in particular for exploring the configuration space of dense systems in the verge of jamming [37]. Our opting for MD resulted from practical considerations (efficiency) and from our concern that short time features (early β relaxation) observed through simple BD could have been misperceived as reliable, while they are not, as a proper BD methodology in our problem requires much more than the simple introduction of a stochastic, "white noise" force. As we discussed in Sec. II, the implementation of appropriate BD for multiarm stars is currently beyond the capability of the technique and the required physical input remains theoretically tentative. Generic questions on a tractable incorporation of hydrodynamic interactions, a proper implementation of the lubrication approximation for "porous objects" and the selection of an appropriate friction coefficient upon intimate approach of soft-spheres precluded efficient mesomodeling.

The major finding of this simulation study is that dense suspensions of soft spheres interacting via potential (ii) [Eq. (2.1)], i.e., our model for multiarm star polymers under marginal solvent conditions, undergo a qualitative change in their dynamics at temperatures higher than 45°C. This is remarkably close to the temperature at which similar phenomena were observed experimentally [5]. The transition is, in a generic sense, a jamming transition. It is caused by the temperature-induced expansion and consequent overcrowding of soft spheres (multiarm star polymers).

There exists abundant simulation evidence in that regard. The radial distribution function exhibits interesting features (split of the second peak and the development of a shoulder in the third peak (Fig. 3). Effects on soft-sphere dynamics are more pronounced. The observed soft-sphere mobility is not consistent with regular Fickian diffusion above 45°C. The α relaxation is apparent in the simulation time scale (Fig. 4). $S_{\rm inc}$ does not scale with q^2t above 45°C (Fig. 7). The self-part of the van Hove correlation function does not evolve

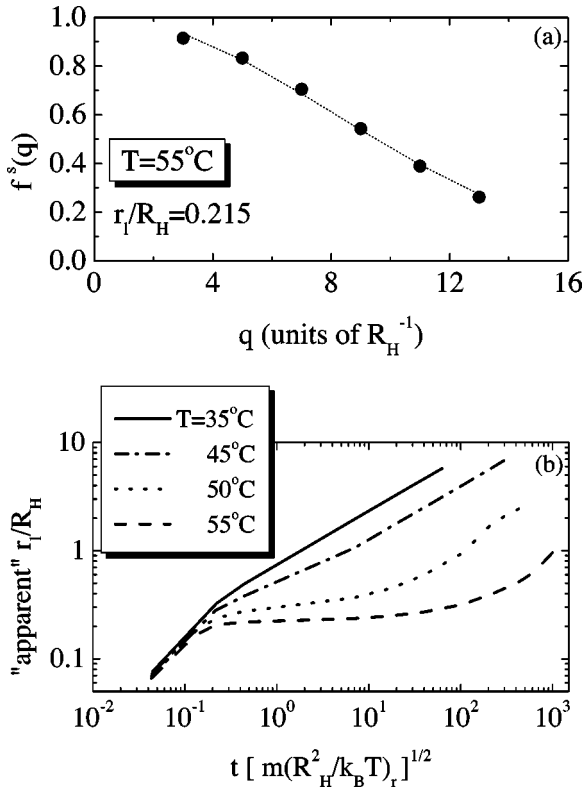

FIG. 13. (a) Fit of the nonergodicity parameter $f^s(q)$ at $T=55\,^\circ$C with $\exp(-q^2r_l^2)$ and estimation of r_l. (b) The localization length r_l vs t at four different temperatures (35, 45, 50, and 55 °C), as it comes from the fit of the incoherent structure factor $S_{\rm inc}(q)$ with the function $\exp(-q^2r_l^2)$.

according to Gaussian statistics (Fig. 5). Individual soft-sphere trajectories (and the MSD in Fig. 4) illustrate the "caging effect" at high temperatures (Fig. 8).

Identified dynamical microclusters are concrete examples of the cooperative nature of soft-sphere self-diffusion (Fig. 9). This is clearly quantified by the displacement-displacement pair correlation function (Fig. 10), which differs from $g(r)$ for distances that extend over several soft-sphere diameters. These differences are especially pronounced for first and second nearest neighbors of the "tagged particle." A characteristic "lifetime" for these correlations was identified in Fig. 11. It is longer than the typical lifetime of cages, and it probably corresponds to the characteristic time for "correlated cage escapes" (see discussion related to Fig. 11 in the previous section).

The incipient transition produces a two step relaxation of $S_{\rm inc}$, i.e., a structural arrest and finite values of the nonergodicity parameter over two decades in the time scale (Fig. 12). The slow relaxation follows von Schweidler's law (Fig. 13). These features are in qualitative agreement with the main predictions of ideal MCT and suggest strongly that our systems are very close to an *ideal glass transition point* (in the *ideal* MCT sense).

The potential employed in the current work [Eq. (2.1)] is an ultrasoft purely repulsive potential. The softness of the potential results in a value of the localization length ($r_1 \simeq 0.22-0.24$; Figs. 4 and 13), which is considerably higher than the corresponding hard sphere value ($0.14R$) [42,45]. However, the major effect of potential softness is not the aforementioned increase of r_1, but the spectacular raise of the nominal volume fraction required for vitrification, which is 1.17 for our soft spheres (see Table I) vs 0.59 for hard spheres [46].

Several theoretical and simulation studies that compare colloidal gels and colloidal glasses have appeared during the past few years [38,42,44,47–50]. From a fundamental point of view colloidal gels are linked to the existence of short range attractive interactions between colloids, which do not exist for the soft-sphere system studied in this work. In this context, the (incipient) nonergodic states of our soft-sphere systems should be viewed as "glasses" rather than "gels." Furthermore, colloidal gels were characterized by a localization length much smaller than that of hard sphere glasses. On the contrary, in our case, the localization length was found to be larger than that of hard sphere glasses. Therefore, on this count too, our soft spheres will form glasses [46].

Stiakakis *et al.* [13] proposed a kinetic phase diagram for dense suspensions of multiarm star polymers in solvents of intermediate quality. According to that phase diagram, "T-induced gels" are characterized by a relatively low concentration, c ($c<c^*$; c^* is the overlap concentration referred to 20 °C, where $R_{\rm H}$ is essentially T independent) and their main feature is that "$T_{\rm gel}$," i.e., the temperature at which dynamical arrest occurs, depends strongly on c (the lower the mass concentration the larger the heating needed to increase the effective volume fraction of the stars and cause jamming). On the contrary, when $c>c^*$, there is hardly any c dependence of $T_{\rm gel}$ and "gelation" is induced primarily by the high original concentration, as the temperature increase causes very little swelling of the stars at such high concentrations. The systems studied in this work fall in the category of temperature induced gels ($c/c^*=0.83$). It is important to point out that the T-induced gels are weaker (lower G') than the c-induced gels [13]; this directly observable difference distinguishes the two classes of gels experimentally. On that basis the T-induced gels could be paralleled to "colloidal glasses," while the c-induced gels to "colloidal gels" [47]. Therefore our soft sphere suspensions form temperature induced gels, which are characterized by weak moduli (akin to colloidal glasses) and a substantial degree of arm interpenetration.

Furthermore, the T-induced gels in Ref. [13] were found to be *ergodic* [5] and exhibited a two-step relaxation of $S_{\rm inc}$ [three step relaxation of the intermediate scattering function, as determined by DLS, which also detects the faster mode of mutual diffusion; Fig. 1(b)]. It should be noted that $S_{\rm inc}$ does not detect mutual diffusion. Clearly, other short-time modes may also exist, which are not captured by the soft-sphere model. This behavior is very similar to the simulation findings on soft-sphere $S_{\rm inc}$ depicted in Fig. 12. In contrast, c-induced gels were clearly nonergodic [13]. It must be noted, however, that the matter of finite nonergodicity factors in the experimental systems is complicated by a very slow yet detectable aging.

Experimental findings point to the existence of distinct "mobile" and "immobile" subpopulations of multiarm stars [5,15]. This situation would have led to a wavelength inde-

pendent plateau of S_{inc}. Experimental data in this respect are suggestive, but not definite [5]. One could distinguish a weak tendency towards a q-dependent plateau, which would argue for caging of all soft spheres. Our simulations support this point of view. Nevertheless, our simulation studies deal with a small population of soft spheres (about 3000). Confocal microscopy has identified mobile and immobile subpopulations at the α-relaxation time scale for hard-sphere colloids [51]. This issue is further complicated by time scale considerations [52]. In our opinion, simulations of tenths of thousands of particles can only address this issue. Furthermore, it should be more usefully addressed to prototype systems (e.g., hard spheres). Further experimental efforts will be valuable in this regard.

V. CONCLUSIONS

We performed a series of MD simulations of concentrated suspensions of soft spheres interacting through the potential of Eq. (2.1), which was designed to mimic the interactions between multiarm star polymers in suspensions under marginal solvent conditions. These studies intended to elucidate the physics underlying the counterintuitive "gelation upon heating" reported experimentally [5].

Simulation findings revealed structural changes (Fig. 3) and, more importantly, features of a prolonged, yet temporal, dynamical arrest of soft-sphere self-diffusion and overall kinetics (Figs. 4 and 10–13). These features conformed to the *ideal* glass transition scenario.

The transition observed in the simulations occurs within 5 °C from the experimentally reported temperature [5]. A two step relaxation of S_{inc} was observed, in agreement with DLS experiments [5]. No finite nonergodicity factors were observed up to $T=55$ °C, again in accordance with DLS measurements [5].

Experimental suggestions of mobile and immobile populations [5] were not corroborated by simulation findings. The tentative nature of these experimental findings, aging complications as well as limitations of the simulation model (lack of appropriate friction) may account for these discrepancies.

It is tantamount that the transition occurs (simulationwise) to within 5 °C from the experimentally reported value, which constitutes a very successful test of potential (ii). According to all simulation findings, it is a jamming transition with reported features of vitrification. The role of temperature is central in these systems, and counterintuititive.

Increasing T speeds up motions, however, it produces soft-sphere expansion and consequent jamming. The competition, as shown by experiments and these simulations, swings in favor of jamming.

ACKNOWLEDGMENTS

Partial support for this work was provided from EU Grant No. HPRN-CT-2000-00017. The authors thank Professor S. H. Anastasiadis for his constructive contribution on the data analysis of S_{inc} and the overall structure of this manuscript.

[1] G. S. Crest, L. J. Fetters, and J. S. Huang, Adv. Chem. Phys. **44**, 67 (1996).
[2] L. L. Zhou and J. Roovers, Macromolecules **26**, 963 (1993).
[3] J. Roovers, L. L. Zhou, P. M. Toporowski, M. v. d. Zwhan, H. Iatrou, and N. Hatzichristidis, Macromolecules **26**, 4324 (1993).
[4] H. Lowen, M. Watzlawek, C. N. Likos, M. Schmidt, A. Jasufi, and A. R. Denton, J. Phys.: Condens. Matter **12**, A465 (2000).
[5] M. Kapnistos, D. Vlassopoulos, G. Fytas, K. Mortensen, G. Fleischer, and J. Roovers, Phys. Rev. Lett. **85**, 4072 (2000).
[6] D. Vlassopoulos, G. Fytas, T. Pakula, and J. Roovers, J. Phys.: Condens. Matter **13**, R855 (2001).
[7] M. Daud and J. P. Cotton, J. Phys. (Paris) **43**, 531 (1982).
[8] T. A. Witten and P. A. Pincus, Macromolecules **19**, 2509 (1986).
[9] T. A. Witten, P. A. Pincus, and M. E. Cates, Europhys. Lett. **2**, 137 (1986).
[10] C. N. Likos, H. Lowen, M. Watzlawek, B. Abbas, O. Jucknischke, J. Allgaier, and D. Richter, Phys. Rev. Lett. **80**, 4450 (1998).
[11] C. N. Likos, H. Lowen, A. Poppe, L. Willner, J. Roovers, B. Cubitt, and D. Richter, Phys. Rev. E **58**, 6299 (1998).
[12] B. Loppinet, E. Stiakakis, D. Vlassopoulos, G. Fytas, and J. Roovers, Macromolecules **34**, 8216 (2001).
[13] E. Stiakakis, D. Vlassopoulos, B. Loppinet, J. Roovers, and G. Meier, Phys. Rev. E **66**, 051804 (2002).
[14] M. Watzlawek, C. N. Likos, and H. Lowen, Phys. Rev. Lett. **82**, 5289 (1999).
[15] G. Fleischer, G. Fytas, D. Vlassopoulos, J. Roovers, and N. Hadjichristidis, Physica A **280**, 266 (2000).
[16] O. Jucknischke, Ph.D. thesis, Westfaelischen Wilhelms-Universitaet Muenster, Germany, 1995.
[17] B. Loppinet, E. Stiakakis, D. Vlassopoulos, and J. Roovers (unpublished).
[18] A. Imhof, A. van Blaaderen, G. Maret, J. Melleme, and J. K. G. Dhont, J. Chem. Phys. **100**, 2170 (1994).
[19] S. E. Paulin, B. J. Ackerson, and M. S. Wolfe, J. Colloid Interface Sci. **178**, 251 (1996).
[20] G. A. McConnel and A. P. Gast, Macromolecules **30**, 435 (1997).
[21] H. Watanabe, T. Kanaya, and Y. Takahashi, Macromolecules **34**, 662 (2001).
[22] I. A. Hamley, C. Daniel, W. Mingvanish, S.-M. Mai, C. Booth, L. Messe, and A. J. Ryan, Langmuir **16**, 2508 (2000).
[23] H. Senff and W. Richtering, J. Chem. Phys. **111**, 1705 (1999).
[24] H. Senff, W. Richtering, C. Norhausen, A. Weiss, and M. Ballauff, Langmuir **15**, 102 (1999).
[25] C. N. Likos, Phys. Rep. **348**, 267 (2001).
[26] A. Jusufi, M. Watzlawek, and H. Lowen, Macromolecules **32**, 4470 (1999).
[27] G. Foffi, F. Sciortino, P. Tartaglia, E. Zaccarelli, F. Lo Verso, L. Reatto, K. A. Dawson, and C. N. Likos, Phys. Rev. Lett. **90**,

238301 (2003).
[28] S. T. Milner, T. A. Witten, and M. E. Cates, Macromolecules **21**, 2610 (1988).
[29] J. Mewis, W. J. Frith, T. A. Strivens, and W. B. Russell, AIChE J. **35**, 415 (1989).
[30] J. N. Israelachvili, *Intermolecular and Surface Forces* (Academic Press, New York, 1985).
[31] D. Vlassopoulos, G. Fytas, S. Pispas, and N. Hadjichristidis, Physica B **296**, 184 (2001).
[32] P. J. Flory, *Statistical Mechanics of Chain Molecules* (Oxford University Press, New York, 1988).
[33] W. Gotze, Condens. Matter Phys. **4**(16), 1 (1998).
[34] W. van Megen, S. M. Underwood, J. Muller, T. C. Mortensen, S. I. Henderson, J. L. Harland, and P. Francis, Prog. Rev. Phys. Suppl. **126**, 171 (1997).
[35] D. Vlassopoulos, G. Fytas, J. Roovers, T. Pakula, and G. Fleischer, Faraday Discuss. **112**, 225 (1999).
[36] H. Lowen, J.-P. Hansen, and J.-N. Roux, Phys. Rev. A **44**, 1169 (1991).
[37] T. Gleim, W. Kob, and K. Binder, Phys. Rev. Lett. **81**, 4404 (1998).
[38] A. M. Puertas, M. Fuchs, and M. E. Cates, Phys. Rev. E **67**, 031406 (2003).
[39] C. Donati, S. C. Glotzer, and P. H. Poole, Phys. Rev. Lett. **82**, 5064 (1999); C. Donati, S. C. Glotzer, P. H. Poole, W. Kob, and S. J. Plimpton, Phys. Rev. E **60**, 3107 (1999).
[40] W. Gotze and L. Sjogren, Rev. Prog. Phys. **55**, 241 (1992).
[41] D. A. McQuarrie, *Statistical Mechanics* (Harper & Row, New York, 1976).
[42] K. Dawson *et al.*, Phys. Rev. E **63**, 011401 (2000).
[43] K. A. Dawson, Curr. Opin. Colloid Interface Sci. **7**, 218 (2002).
[44] A. M. Puertas, M. Fuchs, and M. E. Cates, Phys. Rev. Lett. **88**, 098301 (2002).
[45] M. Fuchs, I. Hofacker, and A. Latz, Phys. Rev. A **45**, 898 (1992).
[46] P. N. Pusey and W. van Megen, Phys. Rev. Lett. **59**, 2083 (1987).
[47] E. Zaccarelli, G. Foffi, K. A. Dawson, F. Sciortino, and P. Tartaglia, Phys. Rev. E **63**, 031501 (2001).
[48] J. Bergenholtz and M. Fuchs, Phys. Rev. E **59**, 5706 (1999).
[49] J. Bergenholtz and M. Fuchs, J. Phys.: Condens. Matter **11**, 10 171 (1999).
[50] J. Bergenholtz, M. Fuchs, and Th. Voigtmann, J. Phys.: Condens. Matter **12**, 6575 (2000).
[51] W. K. Kegel and A. van Blaaderen, Science **287**, 290 (2000).
[52] E. R. Weeks, J. C. Crocker, A. C. Levitz, A. Schofield, and D. A. Weitz, Science **287**, 627 (2000).
[53] M. Stiakakis and D. Vlassopoulos (unpublished).